Dependence of the L-H Power Threshold on X-point Geometry and Divertor Recycling

D.J. Battaglia[1], C.S. Chang[1], S.M. Kaye[1], K. Kim[2], S. Ku[1], R. Maingi[3], R.E. Bell[1], A. Diallo[1], S. Gerhardt[1], B.P. LeBlanc[1], J. Menard[1], And the NSTX Team

[1] *Princeton Plasma Physics Laboratory, Princeton, NJ, USA*
[2] *Korea Advanced Institute of Science and Technology, Daejoen, Korea*
[3] *Oak Ridge National Laboratory, Oak Ridge, TN, USA*

E-mail contact of main author: dbattagl@pppl.gov

Abstract The L-H power threshold decreases with larger X-point radius (R_X) and reduced divertor recycling on NSTX. The edge electron (T_e) and ion temperature (T_i) at the L-H transition are 30% larger for a small R_X shape compared to a large R_X shape, independent of the heating power and divertor recycling. This supports the prediction that a single-particle loss hole, whose properties are strongly linked to R_X and T_i, influences the edge radial electric field (E_r) and $E_r \times B$ flow-shearing rate available for turbulence suppression. Simulations using XGC0, a self-consistent full-f drift-kinetic neoclassical code, indicate that achieving the same $E_r \times B$ flow-shearing rate at the L-H transition does require about 30% larger edge temperature as R_X decreases. The calculations also demonstrate that more heating power is needed to achieve the critical edge T_i for a given magnetic geometry and edge density as the contribution of divertor recycling to the total neutral fueling increases.

1. Introduction

Most existing and planned magnetic fusion devices, such as ITER [1], are designed to operate in the high-energy confinement or H-mode regime [2]. This regime features a broad core pressure profile leading to improved magneto-hydrodynamic (MHD) stability, and a large edge pressure gradient that allows the plasma temperature in contact with the wall to be low while the core temperature is high. The transition from a low-confinement (L-mode) to H-mode regime is attributed to an abrupt reduction in the radial transport near the plasma edge. The transport suppression mechanism remains under investigation, but leading theories include the decorrelation of turbulent eddies via mean $E_r \times B$ flow shear [3] or the interaction of mean and turbulent driven $E_r \times B$ flow shear [4], where E_r is the edge radial electric field and B is the local magnetic field. In both theories, sufficient $E_r \times B$ flow shear near the plasma edge is needed to initiate and sustain H-mode.

Achieving H-mode requires sufficient plasma heating such that the power lost through the plasma boundary exceeds a threshold (P_{LH}) [5]. Predicting and controlling P_{LH} is important for the design and operation of future tokamak reactors. A number of experiments have observed that P_{LH} varies with the position of the X-point and divertor conditions [6]. Section 2 of this article reports recent experiments on the National Spherical Torus Experiment (NSTX) that document the variation in P_{LH} versus the X-point radius (R_X) over a wide range of fueling and divertor recycling regimes. The significant observation is that the edge ion and electron temperatures at the time of the L-H transition are fairly insensitive to the loss power and divertor recycling regime, but increase as R_X decreases. In Section 3, predictions derived from the X-transport theory [7] are shown to be consistent with the experimental observations. A full-f drift-kinetic neoclassical simulation code (XGC0) that captures the important X-transport and neutral fueling physics is shown to reproduce the experimental observation of a critical edge ion temperature that depends on R_X, but is insensitive to divertor recycling.

2. P_{LH} Dependence on R_X and Divertor Pumping

Data from the first experiments at NSTX to demonstrate the dependence of P_{LH} on R_X are presented in [8], however the analysis was complicated by large variations in $dW/dt + P_{OH}$ where dW/dt is the change in the plasma stored energy and P_{OH} is the resistive heating power. The new data reported in this paper remove that uncertainty by delaying the L-H transition to a time in the discharge with nearly stationary $dW/dt + P_{OH}$, and repeating the experiment over a range of divertor recycling conditions. Preliminary analysis of the present dataset is presented in recent overview papers [9].

The magnetic boundaries of the two discharges used in the experiment are shown in Fig 1. The boundaries are computed using an equilibrium reconstruction derived from magnetic data and an isothermal T_e constraint at the midplane [10]. One discharge has R_X = 0.66m, i.e. large R_X or low triangularity, while the other discharge has R_X = 0.49m, i.e. small R_X or high triangularity. The discharges have matched plasma current (I_P = 0.8 MA) and on-axis toroidal field (B_{T0} = 0.55 T) in the favorable ∇B configuration (ion grad-B drift is down). The discharges also have a similar X-point height, plasma surface area, inner and outer gap, and magnetic axis radius. The two discharge shapes were reproduced under three divertor recycling and neutral fueling conditions: (1) low divertor recycling and large neutral gas fueling rate, (2) high divertor recycling and low neutral gas fueling rate and (3) high divertor recycling and medium neutral gas fueling rate. The low recycling divertor is achieved on NSTX by evaporating fresh solid lithium on the divertor surfaces, while the high recycling divertor has passivated lithium coatings.

For all of the discharges in this dataset, a 20 – 30 ms stationary L-mode discharge was established with only inductive ohmic heating before adding auxiliary heating. The P_{LH} was identified for each condition by running a series of discharges with incrementally larger neutral beam injection (NBI) heating until a long (> 30 ms) H-mode was observed no earlier than 50 ms (a few fast ion slowing down times) after the start of the NBI. The minimum NBI power (P_{NBI}) needed to access H-mode for each shape in three different fueling scenarios is shown in Fig 2a. P_{NBI} is the lowest for the low recycling divertor (squares) for both shapes. For the other two scenarios with a high recycling divertor, the discharges with the lower neutral fueling rate (triangles) have a smaller P_{NBI} than the discharges with the larger neutral fueling rate (diamonds). For each fueling scenario, the small-R_X (high triangularity) shape requires more neutral beam heating power to achieve H-mode. The loss power at the L-H transition ($P_{LH} = P_{heat} + P_{OH} - dW/dt$) for each discharge at the time of the L-H transition is calculated using TRANSP simulations (Fig 2b). The trends of P_{LH} are similar to P_{NBI}, albeit the differences are less pronounced, with a P_{LH} for the small-R_X shape that is about 30% larger for each fueling scenario. The error in P_{LH} is approximated to be 15%, with a majority of the uncertainty due to systematic error in calculating the beam heating efficiency.

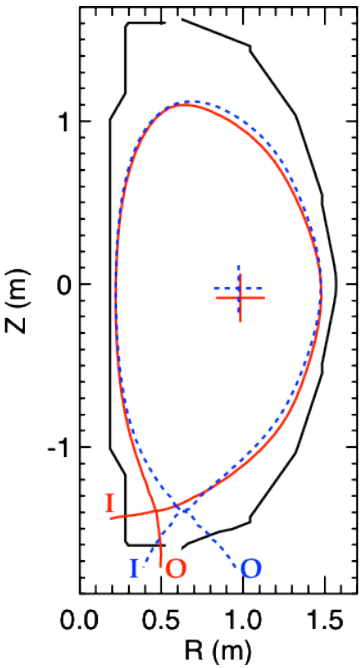

FIG. 1. Plasma separatrix for small-R_X (solid red) and large-R_X (dotted blue) shapes. Crosses indicate position of magnetic axis.

The electron density (n_e) and temperature (T_e) profiles at the midplane are measured using a Multi-pulse Thomson Scattering system. The L-mode profiles are slowly evolving (both n_e and T_e are increasing < 20% every 17 ms). The n_e profile has a pedestal that can be fit with a hyperbolic tangent function [11]. The height of the n_e pedestal for the last L-mode profile is shown in Fig 2c, while the corresponding line-integrated density is shown in Fig 2d. Note that the first two fueling scenarios (squares and triangles) have similar L-mode line-integrated n_e but different levels of divertor pumping. In this comparison, the strong pumping from lithium coatings decreased P_{LH} by about 20%. The third fueling scenario (diamonds) was operated at a higher line-integrated density, but matches the pedestal density of the low recycling divertor (squares), leading to a near doubling of P_{LH}.

Figure 3 shows a number of L-mode profiles for the matrix of six discharges. In Fig 3a, the n_e profiles are normalized to the pedestal height and aligned relative to the pedestal symmetry point. The gray vertical box indicates a typical range of the radial location of the separatrix. The hyperbolic tangent fit for the data has a width of 1.5cm ($\Delta\psi_N \sim 0.045$). Figure 3b shows the T_e profiles for the same six discharges. For each shape, the edge T_e profile is similar despite a large range in the NBI heating (see Fig 2a). This gives the impression of a critical edge temperature that is independent of the divertor recycling and core heating. However, this critical edge temperature depends on R_X, as the T_e at the top of the density pedestal (–2 cm) is 30% larger for the small-R_X shape than the large-R_X shape. This is consistent with the 30% difference in P_{LH} for the two different shapes.

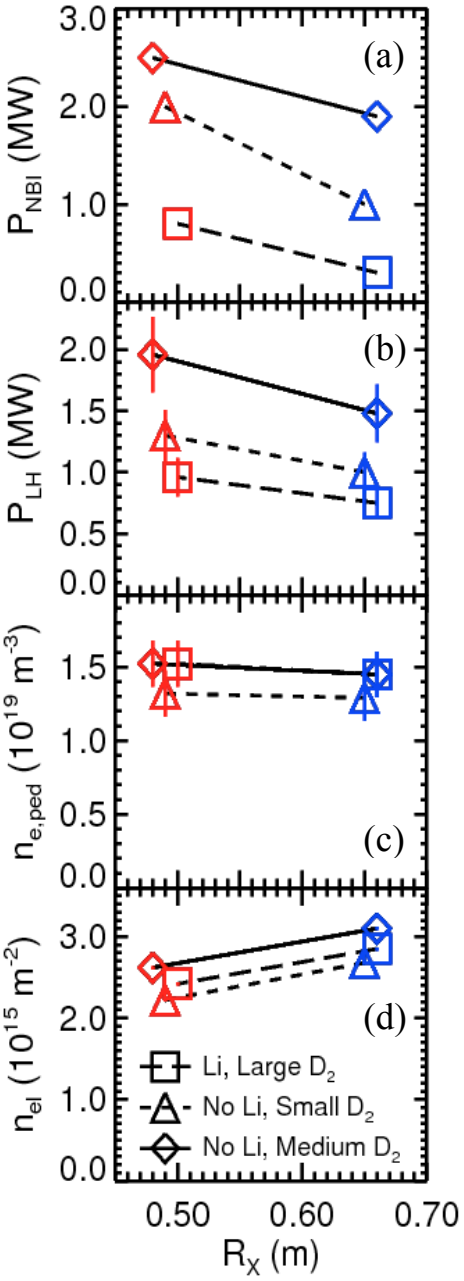

FIG. 2. (a) P_{NBI}, (b) P_{LH}, (c) pedestal n_e and (d) line-averaged n_e versus R_X for different neutral fueling scenarios.

A direct measurement of the L-mode edge ion temperature (T_i) is difficult due to poor carbon confinement in L-mode, hindering both passive and active CVI charge-exchange spectroscopy measurements near the edge. Figure 3c shows the active CVI measurements with least squares linear fit of the data for each experimental shape. The linear fits are also over-plotted on Fig 3b as dotted lines. While the measurements were insufficient to constrain the local T_i in the edge region, the extrapolated core measurements suggest $T_i \sim T_e$. This assumption is reasonable considering that the thermal equilibration of the main ions and electrons is on the order of a few milliseconds when T_e < 100 eV [12],

which is several times shorter than the local electron thermal confinement time in the edge region for typical L-mode NSTX discharges.

The following conclusions are derived from these data: (1) P_{LH} increases as R_X decreases (triangularity increases) for a large range of fueling a pumping scenarios, (2) the edge T_e (~ T_i) near the time of the L-H transition is weakly dependent on the core heating, divertor pumping and fueling conditions, but increases as R_X decreases, and (3) the core heating needed to achieve the critical edge conditions increases as the divertor recycling increases. It is important to consider that moving R_X also changes the strike point positions and the nature of the recycling in the divertor. While, it is therefore difficult to decouple the relative impact of R_X and divertor recycling on P_{LH}, the dependence of the critical edge temperature on R_X appears to be insensitive to changes in the divertor recycling while having a strong dependence on R_X.

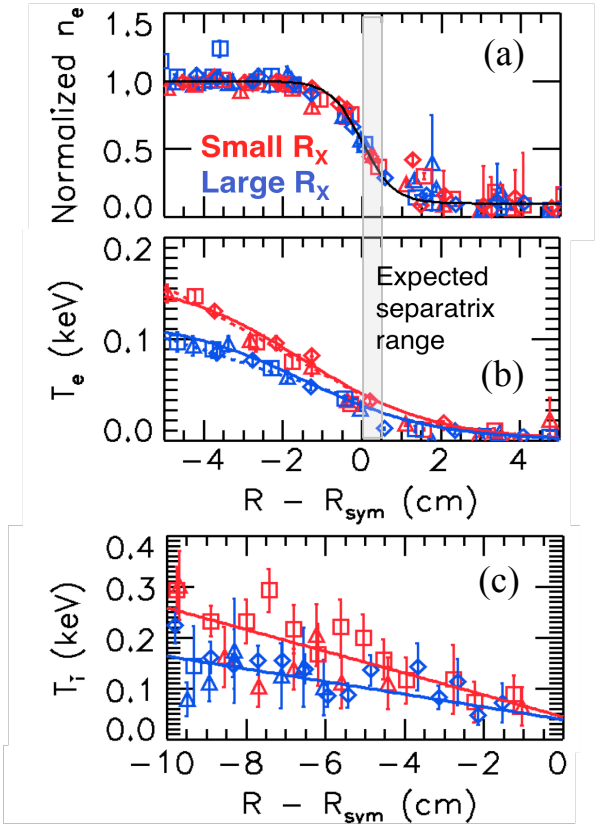

FIG. 3. (a) n_e / n_{eped}, (b) T_e, and (c) T_i near the L-H transition for the six discharges

3. Self-consistent Full-f Neoclassical Simulations of the L-mode Edge

These experimental conclusions support the predictions derived from the kinetic neoclassical description of the plasma edge in a diverted tokamak [7]. The rationale of the theory is that a single particle orbit loss hole for flux surfaces near plasma edge can lead to neoclassical plasma transport that is not automatically ambipolar. This source of non-ambipolar transport, called X-transport, impacts E_r near the plasma boundary and is strongly dependent on R_X and is function of T_i [7,13,14].

The impact of R_X on the loss hole is illustrated here using a single particle guiding center model in the absence of any electric fields, collisions or flows [15]. In these conditions, the lowest energy loss orbits are trapped ions that originate from the outboard midplane ($R > R_0$ and $d\psi/dz = 0$) and are lost to the inner divertor leg when $\nabla B \times B$ is pointing toward the X-point (favorable ∇B configuration). Higher energy ions on passing orbits can be lost to the outer divertor leg. The velocity space loss hole in pitch-energy space for ions launched at $\psi_N = 0.96$ ($\Delta r = 1.05$ cm from separatrix) at the outboard midplane of the two NSTX shapes are shown in Fig 4. The position of the launch location (Δr) along the midplane is near the top of the pedestal region; however, the launch depth is arbitrary in this model since the energy axis scales approximately as Δr^2 [13]. Counter going ions launched with pitch and energy components in the unshaded region are either confined passing or trapped orbits (regions labeled P and T, respectively). The loss hole

(shaded region) is divided into two regions: the lower-energy ions lost to the inner (I) divertor leg and the higher-energy ions lost to the outer (O) divertor leg.

The vertical arrows in Fig 4 indicate the minimum unconfined ion energy (K_0) for the two different plasma shapes. The K_0 for the large-R_X shape is 71 eV (Fig 4a and blue arrow), while the K_0 for the small-R_X shape is 96 eV (Fig 4b and red arrow), which is 35% larger. The reduction in K_0 with R_X is due to (1) longer ion bounce orbits prior to entering the X-point region and (2) lower B_Z shear in the X-point region. The large-R_X shape also has a larger loss region above K_0 compared to the small-R_X shape since more trapped orbits have bounce points inboard of the X-point. The relative differences in the loss holes, including the 35% difference in K_0, are the same for all points along the midplane in the edge region ($\psi_N > 0.85$). The number of ions in the distribution tail that reside in the loss hole is related to T_i.

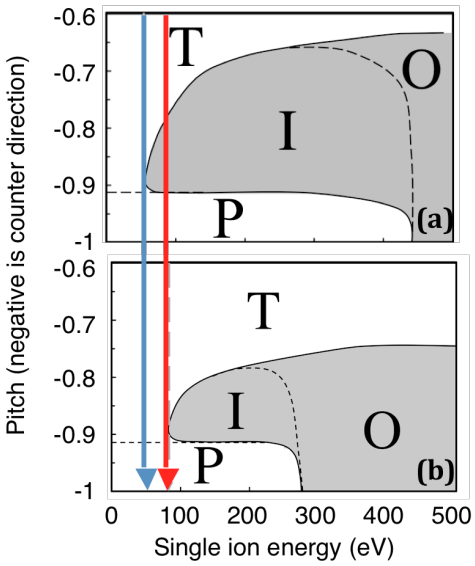

FIG. 4. Ion velocity loss hole at Ψ_N = 0.96 on the outboard midplane for (a) large-R_X shape and (b) small-R_X shape. Arrows indicate critical loss energy. Note suppressed vertical axes.

The change in the loss holes with R_X is consistent with the observed dependence of the critical edge T_i on R_X. For matched L-mode profiles, the large-R_X (low triangularity) shape will have a larger level of X-transport, and consequently a more negative E_r inside the separatrix, compared to the small-R_X shape. This leads to a larger degree of $E_r \times B$ flow shear, which is believed to be important in initiating and sustaining the L-H transition. One way to match the $E_r \times B$ flow shear for the two shapes is to increase the heating, and thus increase the edge T_i, for the small-R_X shape.

This argument is illustrated using self-consistent calculations of E_r and $E_r \times B$ flow shear from the XGC0 code [16]. This code solves the single particle drift-kinetic equations for many (~10 million) particles for an experimentally measured MHD equilibrium. The presented simulations only follow neutral and ionized deuterium in the electron background. A good match to the L-mode experimental profiles is achieved when a random anomalous particle diffusion of 0.05 m^2/s is added to account for ambipolar diffusion from turbulent transport. All simulations have a recycling coefficient of unity, such that any particle that intersects a wall is reborn as a neutral atom particle. Heat and torque are applied at the core boundary in order to achieve stationary profiles.

The calculated equilibrium n_i (more correctly, the guiding center density $n_{i,gc}$), T_i and ion $v_{//}$ profiles are shown in the left hand column of Fig. 5. The red and blue lines show the simulation results for the small-R_X and large-R_X shapes where core heating and torque are matched. In these cases, the density, temperature and parallel flow profiles are similar. The green traces are the results for the small-R_X shape where the core heating and torque were increased by 30%, resulting in larger temperatures and parallel flows for the same density.

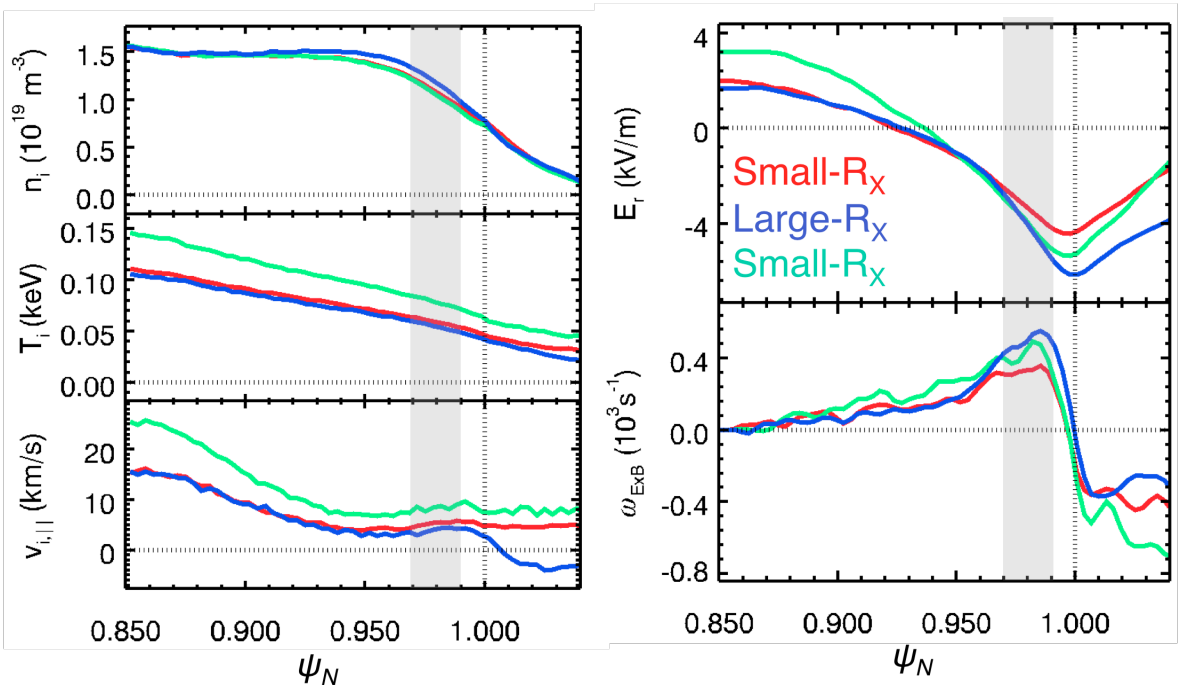

FIG. 5. XGC0 simulations of small-R_X (red) and large-R_X (blue) with matched core conditions. A simulation with the small-R_X shape and core heating and torque increased by 30% (green) gives a better match to the maximum shear rate of the large-R_X shape.

The corresponding E_r and $E_r \times B$ shearing rate [3] profiles for the three simulations are shown in right hand column of Fig. 5. The large-R_X shape (blue) has a deeper E_r well for $\psi_N > 0.97$ than the small-R_X simulation with matched core boundary heat and torque flux (red). Consequently, the E_r x B shear rate achieves a larger peak for the large-R_X shape. When the core heating and torque flux are increased by 30% for the small-R_X shape (green), the E_r well becomes deeper and the peak shear rate for $\psi_N > 0.97$ nearly matches the lower power large-R_X shape. Therefore, if the L-H transition requires a critical E_r x B shear rate, then the simulation results support the experimental observation that 30% more NBI heating is needed to achieve the L-H transition.

The influence of the ion loss hole is seen the equilibrium ion distribution function for particles inside a toroidal ring at the outboard midplane (Fig. 6). E_r is driven negative until the confinement of high-energy ions is improved such that the loss of counter-I_p ions is balanced by a pinch of co-I_p ions. This leads to a non-Maxwellian ion distribution where the mean parallel flow is "intrinsically" in the co-I_p direction [17]. The resulting co-I_p flow layer just inside the separatrix can be seen in the flow profiles shown in Fig 5.

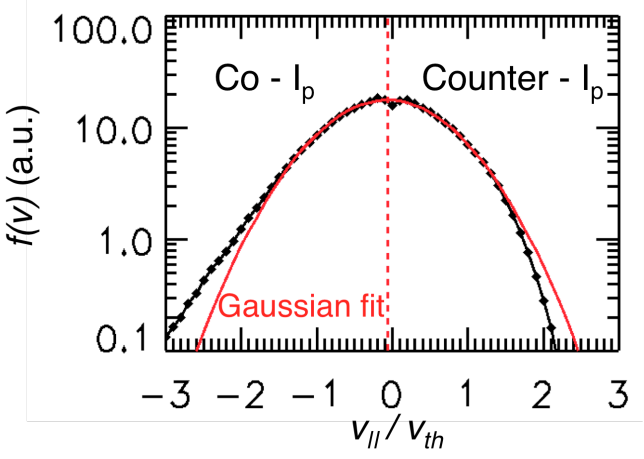

FIG. 6. Calculated $v_{//}/v_{th}$ distribution for the ions in a toroidal ring: $0.99 < \psi_N < 1$ and $-10° < \theta < 10°$.

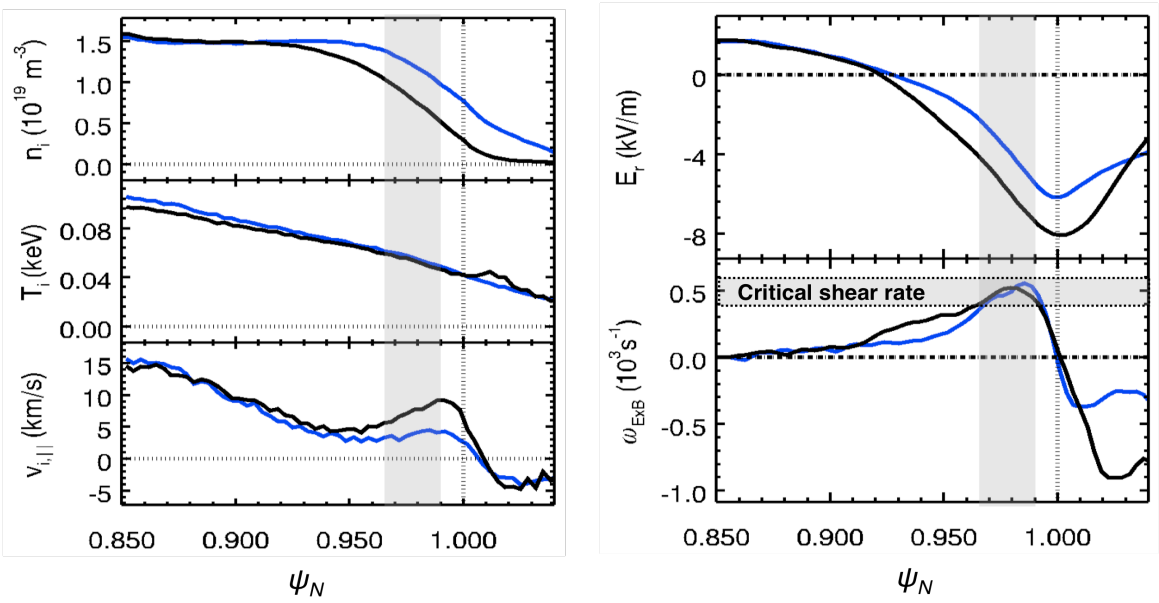

FIG. 7. XGC0 simulations of large-R_X shape with a high recycling (blue) and low recycling (black) divertor with 20% less core heating and torque input.

The changes in E_r due to changes in the divertor recycling are investigated by using two different recycling models in XGC0. The results shown in Fig 5 used a model where a neutral particle is born from the location where an ion was lost to the wall. This is typical of a high recycling divertor where most of the neutral fueling comes from the divertor. In a lower recycling divertor, the density is maintained by external neutral fueling during L-mode and the neutral density is more evenly distributed throughout the SOL. To simulate a lower recycling divertor, a neutral lost to the wall is reborn on a random position on the wall. A detailed comparison of these two models is reported in [18]. In Fig 7, the profiles for simulations using the two models are shown. The solid blue is the same results shown in Fig 5 for the large-R_X shape with a high recycling divertor. The black profiles are for the same shape with the low recycling divertor model and the core heating and torque reduced by 20%. The lower recycling divertor has a density profile that is shifted inward and a more peaked edge flow layer. When the neutrals are distributed throughout the SOL, the fueling efficiency and penetration depth are improved; consequently, a lower neutral density at the separatrix is needed to maintain the core density. This reduces the charge exchange losses in the ion channel, reducing the core heat flux needed to achieve a certain edge ion temperature.

The experimental results found a nearly 100% reduction in P_{LH} when lithium was used to reduce the divertor recycling while maintaining a constant pedestal density via neutral fueling. Therefore, the 20% reduction in the simulation achieves the correct trend, but under predicts the experimental result. A more localized gas puff model, together with the addition of kinetic electrons and impurity species may improve the quantitative match. These capabilities already exist in XGC0, but not used in the present study.

4. Conclusion

The data and modeling presented in this paper lends strong support for the theory that an ion velocity loss hole influences the edge E_r in L-mode and thus the $E_r \times B$ flow shear available to initiate the L-H transition. In addition to R_X, the critical energy and size

of the ion velocity loss hole is predicted to scale with parameters that are known scalings of P_{LH} in tokamaks. This includes the $\nabla B \times B$ direction, aspect ratio, I_p, ion mass (M_i), effective charge (Z_{eff}), toroidal loop voltage and plasma elongation. Therefore, the contribution of the ion velocity loss hole to the edge E_r may describe some of the "hidden variables" in the P_{LH} scaling relation. Looking ahead, the predictions of X-transport can be exploited to reduce the heating power demands of future tokamaks. For example, a discharge could start with a large R_X to facilitate H-mode access at lower heating power, and then shift R_X to smaller values while in H-mode to optimize MHD stability and the achievable density relative to the Greenwald density limit scaling. Also, the role of the edge T_i in establishing the necessary $E_r \times B$ flow shear for the L-H transition highlights the importance of minimizing the penetration of recycled neutrals from the divertor. Future computational and experimental work will focus on quantifying the relationship between the E_r and the edge profiles, especially T_i, in light of the predicted ion velocity loss hole.

This work was funded by the US Department of Energy under Contract Numbers DE-AC02-09CH11466 and DE-AC05-00OR22725. This research used resources of the National Energy Research Scientific Computing Center, which is supported by the Office of Science of the U.S. Department of Energy under Contract No. DE-AC02-05CH11231.

---

[1] SHIMADA, M., et al., *Nucl. Fusion*, **47** (2007) S1-S17

[2] WAGNER, F., et al., *Phys. Rev. Lett.* **49** (1982) 1408-12

[3] BURELL, K.H., *Phys. Plasmas*, **4** (1997) 1499-518

[4] CONWAY, G.D., et al., *Phys. Rev. Lett.* **106** (2011) 065001

[5] MARTIN, Y.R., et al., *J. Physics: Conf. Series* **123** (2008) 012033

[6] ANDREW, Y. et al., *Plasma Phys. Control Fusion* **46** (2004) A87
KALUPIN, D. et al., *Contrib. Plasma Phys.* **50** (2010) 356
CARLSTROM, T.N. et al., *Fusion Sci. Technol.* **48** (2005) 997
GOHIL, P. et al., *Nucl. Fusion* **51** (2011) 103020

[7] CHANG, C.S., et al., *Phys. Plasmas*, **9** (2002) 3884-92

[8] MAINGI, R., et al., *Nucl. Fusion* **50** (2010) 064010

[9] KAYE, S.M., et al., *Nucl. Fusion* **51** (2011) 113019
RAMAN, R., et al. *Nucl. Fusion* **51** (2011) 094011
HAWRYLUK, R.J., *Nucl. Fusion* **51** (2011) 094005

[10] MENARD, J.E., et al., *Phys. Rev. Lett.* **97** 095002

[11] GROEBNER, R.J., and OSBORNE, T.H., *Phys. Plasmas* **5** (1998) 1800-6

[12] NRL Plasma Formulary, NRL/PU/6790-02-450

[13] CHANKIN, A.V., and McCRAKEN, G.M., *Nucl. Fusion* **33** (1993) 1459-69

[14] MIYAMOTO, K., *Nucl. Fusion* **36** (1996) 927-38

[15] KU, S., et al., *Phys. Plasmas*, **11** (2004) 5626-33

[16] CHANG, C.S., et al, *Phys. Plasmas* **11** (2004) 2649-67

[17] DeGRASSIE, J.S. et al., *Nucl. Fusion* **52** (2012) 013010

[18] STOTLER, D.P. et al., *J. Nuclear Materials, submitted (2012)*